Adequacy of quantitative interpretation and use of additional data required for correlation, calibration, and integration

Bill Goodway[1]

ABSTRACT

Quantitative interpretation (QI) is a buzz word these days, but generally falls short of the expectations seismic interpreters have for its applications. This happens because QI is indeed an ambitious ill-constrained goal but can be achieved with adequate calibration. The discussion in this paper focuses on the adoption of some additional under-utilized supplementary data that are needed for correlation, calibration and integration in the context of successful application of appropriate AVO/QI workflows. These include, *first,* the walkaway AVO VSP and elastic logs for combined borehole and surface seismic inversion after utilizing the VSP guided background offset scaling/balancing. The resulting elastic properties derived through AVO inversion show higher correlations with the log data. *Second*, the use of error free elastic logs for AVO calibration and rock physics modeling is crucial, as the detection of errors and their interpretation could be misleading and a waste of precious time. *Third*, an accurate low-frequency model is required for performing AVO inversion and deriving the elastic properties therefrom. This could include well log co-kriged migration velocities or the use of FWI velocities. *Finally*, the use of accurate angle-dependent wavelets is required for AVO impedance inversion, which are usually extracted under an isotropic assumption. An overlooked issue concerns the background shales with VTI anisotropy, which is not accounted for. If such additional data are utilized for AVO inversion and brought into the QI exercises, the results would be encouraging.

KEYWORDS

Quantitative interpretation, AVO, walkaway VSP, FWI velocities, low-frequency model, angle-dependent wavelets, anisotropy

INTRODUCTION

Quantitative interpretation (QI) has become a buzz word in our industry over the last decade. Besides adopting appropriate workflows, additional data are required for correlation, calibration and integration. However, quite frequently, a question that arises in the minds of seismic interpreters is if it is really being done effectively, or is it just a buzz word?

I address this question in the context of AVO inversion of seismic data. To remotely describe the subsurface in all its geological complexity of lithology, porosity, rock fabric, fluids, pore pressure and in-situ stress is arguably the sole goal of applied geophysics. Consequently, in order to meet this ambitious goal of inverting seismic data for QI, it requires wide-ranging and comprehensive inclusion of supplementary data from a variety of sources such as borehole logging, petrophysics, rock physics, core measurements, lithofacies description and processing velocities, etc.
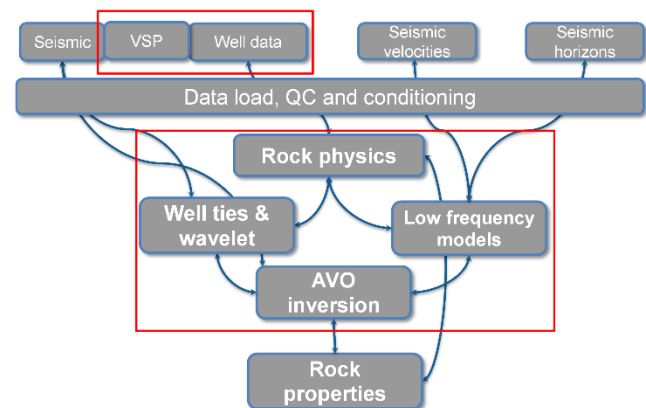

Figure 1: Typical workflow for AVO/QI.

This paper focuses on some additional under-utilized supplementary data that are needed for correlation, calibration and integration for the successful application of appropriate AVO/QI workflows as shown in the red boxes in Figure 1 for a general AVO inversion flow diagram loop. My suggestion is that if four essential changes are adopted in the workflow, the results would be far more promising. These are (1) QI confirmation/calibration of walkaway AVO VSP and elastic logs for combined borehole and surface seismic inversion: walkaway VSP guided background offset scaling/balancing, (2) necessary error free full elastic log suite for AVO calibration and rock physics modelling, (3) need for correct LFM low frequency models for AVO Fluid Factor and QI from relative and absolute Inversion: well log co-kriged with migration velocities or Full

[1] Qeye Labs, Calgary. Emails: bg@qeye-labs.com;

Waveform Inversion (FWI) velocities, and (4) wavelet estimation including VTI log tie - both spectral amplitude and phase-) and wavelet spatial estimation/stability especially for phase.

ADDRESSING QI ADEQUACY

I will elaborate on each of the above-mentioned points below and make the case that they result in value-addition to the QI exercises when adopted carefully and responsibly. I begin with the first one as follows.

1.   QI confirmation/calibration of walkaway VSP AVO and elastic logs for combined borehole and surface seismic inversion: walkaway VSP guided background offset scaling/balancing

The ability to accurately invert for elastic parameters to predict lithology and fluid type from surface seismic, is greatly affected by the quality of prestack AVO amplitudes that are degraded by noise and multiple interference. Consequently, the degree to which prestack processing preserves the AVO response is generally unknown and a "true" AVO measurement, free of noise and multiple contamination, is needed to calibrate surface data for quantifiably reliable inversion results.

A rarely used walkaway VSP can provide a noise/multiple free seismic measurement to calibrate and condition the surface seismic AVO, as well as providing true amplitude evidence of a quantifiable AVO response (Coulombe et al., 1996; Goodway et al., 1998; Downton et al., 1999; Goodway, 2001).

Figure 2a shows the walkaway VSP geometry designed for AVO analysis and calibration. Source and receiver locations are schematically shown by flags and triangles respectively with the 7 source half-offsets located from 50 m to 850 m being equivalent to 100 m to 1700 m in two-way reflection offset. An amplitude preserving processing flow applied to both VSP and collocated 3D surface data, was guided and calibrated by a joint log AVO synthetic and offset VSP method. The resulting "true" VSP reflectivity "AVO gather" response shown in Figure 2b, establishes and confirms the AVO expectation for a class III AVO gas sand at 0.95 s two-way-time (TWT).

A further use of the VSP "AVO gathers", is the identification of internal multiple interference along with its AVO response as a result of being generated from the overlying sand AVO and coal reflections' multipathing below the lowest borehole receiver level (Figure 2b).
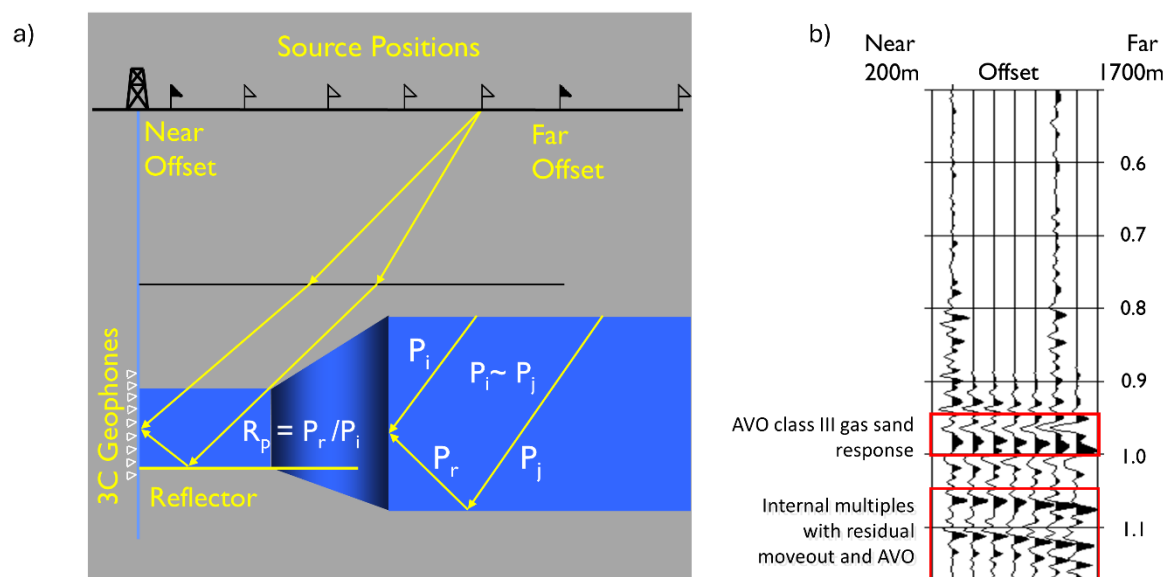

Figure 2: (a) Geometry adopted for the walkaway VSP data acquisition. (b) AVO gather from VSP PP reflections. Notice the AVO expectation for a class III gas sand in the gather at 0.95 s, as well as the later arriving internal multiple interference that also exhibits an AVO response.

A collocated surface 3D processed through a VSP controlled AVO preserving workflow, facilitates a direct calibrated and quantified comparison of the reliability of various AVO simultaneous inversion estimates for P-impedance, S-impedance and Lambda-Rho. Simultaneous inversion uses multiple offset or angle seismic sub-stacks and their associated wavelets as input to output P-impedance, S-impedance or V_P/V_S, Lambda-Rho, Mu-Rho and density. For each input partial stack, a unique wavelet is estimated (see section 4). These partial stacks and wavelets are input to the inversion algorithm that effectively compensates for offset-dependent phase, bandwidth and tuning effects. The algorithm works by first estimating angle-dependent P-wave reflectivities for the input-partial stacks that are then modeled and fitted with approximations to the full Zoeppritz equations such as the Aki-Richards equation to find band-limited elastic reflectivities.

Figure 3 compares ground truth log data tied to these inverted elastic parameters from the 3D and P-P and P-S converted wave VSP outputs. Qualitatively the inverted 3D and VSP traces have a reasonable match for P-impedance and S-impedance, with the Lambda-Rho (Figure 3c) showing a considerably improved match to the log ground truth especially at the Viking target.

The inverted 3D surface seismic and VSP data, when tied directly to well logs in depth and time, quantify the correlation of basic P-impedance and S-impedance inverted traces to wireline logs as shown in Figures 4a, and 4b. This dataset's comparison with log data for P-impedance shows excellent correlation values of 0.85 for the surface 3D (Figure 4a), 0.9 for the walkaway VSP (Figure 4b) and 0.97 for the VSP corridor stack (Figure 4c).
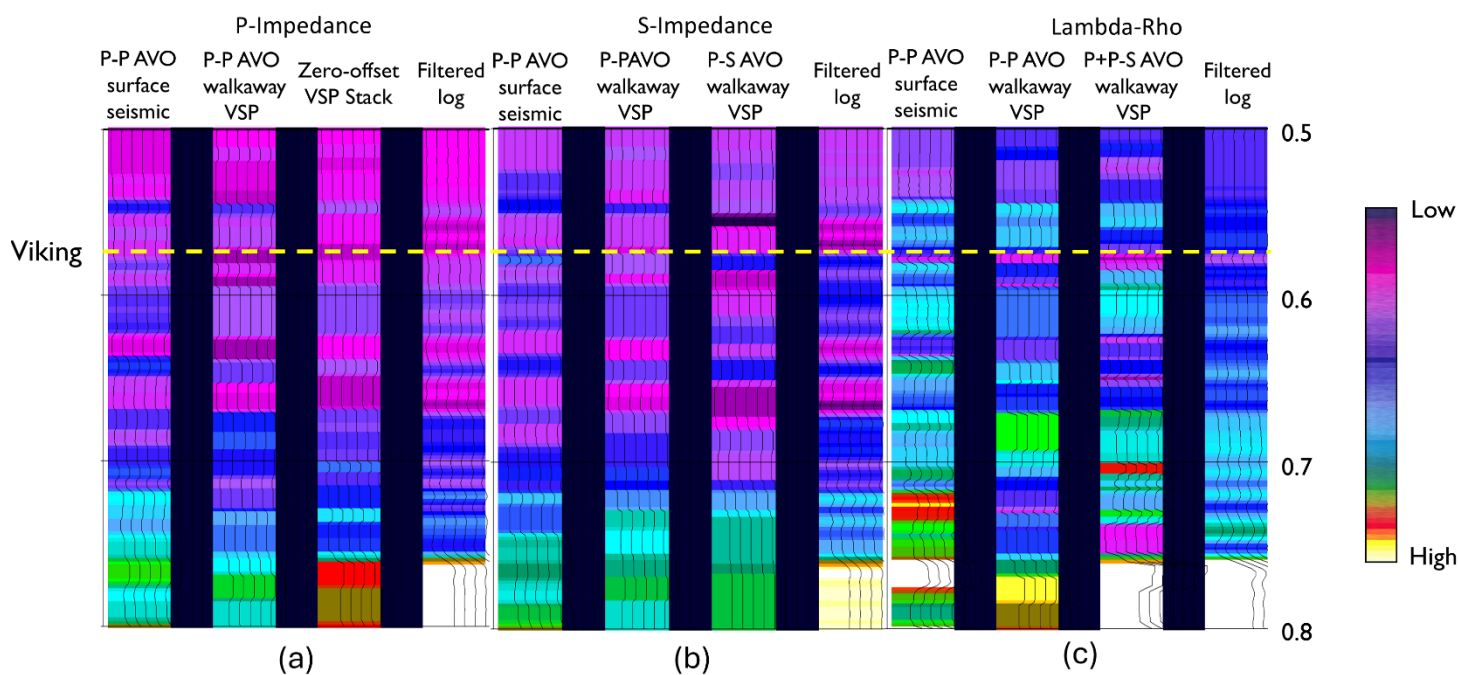

Figure 3: Comparison of VSP to surface seismic inversions and with well log information comprising (a) P-impedance, (b) S-impedance, and (c) Lambda-Rho. Notice, the inverted seismic and VSP traces exhibit a reasonable match with P- and S-impedance, but an improved match is seen with Lambda-Rho.
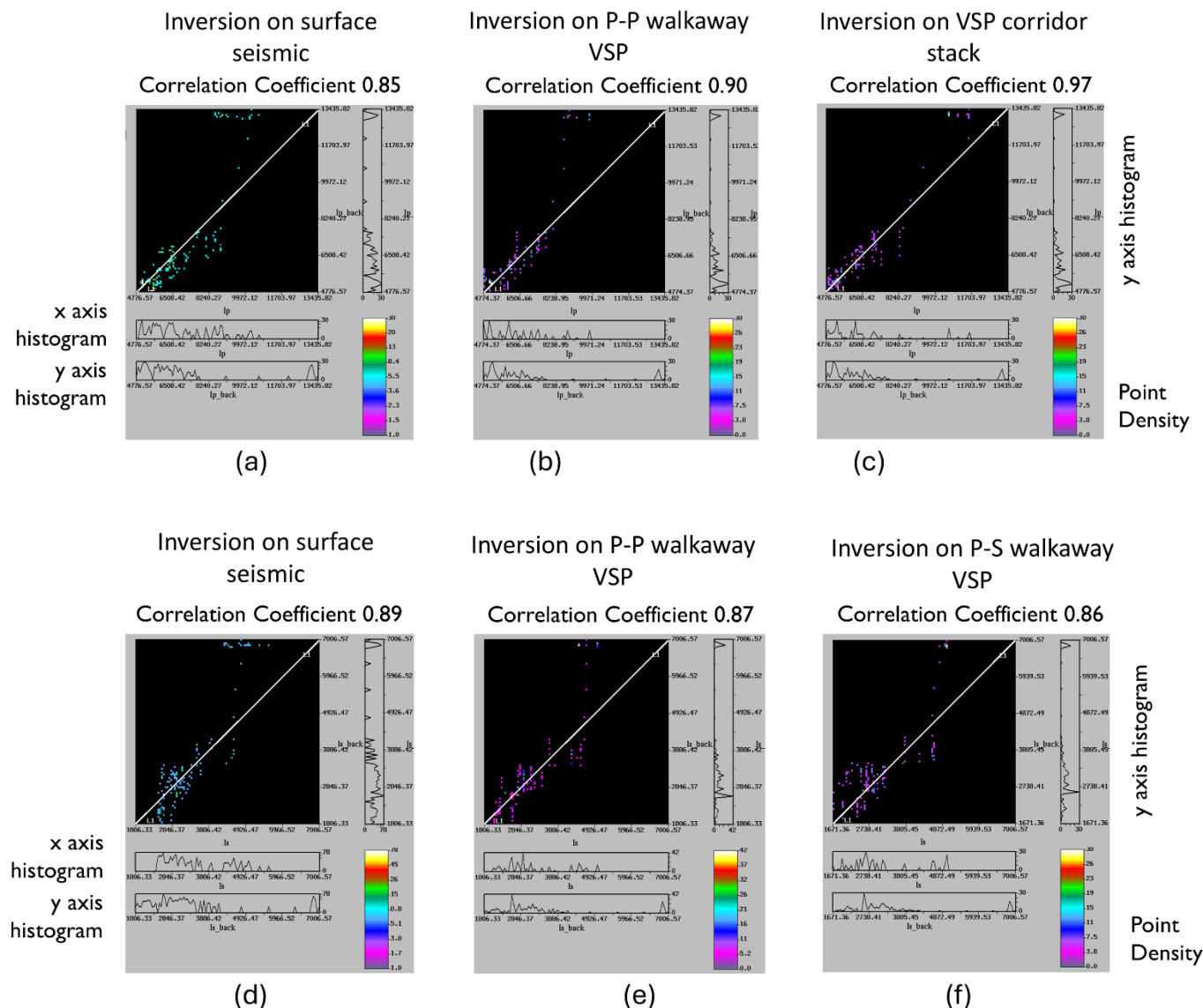
Figure 4: Crossplotting of measured and inverted P-impedance for (a) surface seismic data, (b) walkaway VSP data, and (c) VSP corridor stack. Similar S-impedance crossplots are shown for (d) surface seismic data, (e) PP walkaway VSP data, and (f) PS walkaway VSP data. High correlation coefficients are seen for all the crossplots.

The comparison for S-impedance with log data shows a slightly better correlation of 0.89 for the 3D surface seismic (Figure 4d), with slightly lower correlations of 0.87 for the P-P walkaway VSP (Figure 4e) and 0.86 for P-S converted wave walkaway VSP (see Figure 4f). These high correlations between the various inverted elastic properties and log values demonstrate the need and benefit of using the walkaway VSP to calibrate and control both the amplitude preserved processing and AVO inversion.

2. Necessary error-free full elastic log suite for AVO calibration and rock physics modelling

The importance of having a full suite of P-wave, shear and density logs for litho- and poro-elastic facies ground truth calibration in AVO/QI is well recognized, and most projects fulfill some basic requirement for elastic logs. However, a critical yet often overlooked need is for edited and error-free shear sonic and sonic scanner anisotropic tensor solution logs. This is particularly true for shear logs, where insufficient

4

correlation length can lead to unstable synthetic log ties. Such limitations lead to flawed low frequency background reference models (LFM), depth trends and synthetic seismic angle wavelet ties, that significantly diminish the accuracy of QI.

Hidden sonic log errors, especially for shear measurements, are frequently missed due to an inadequate understanding of how to analyze and identify these errors. Figures 5 and 6 illustrate an example of log-based error identification analysis, that compare Castagna and Smith's (1994) published world-wide logs plotted as P impedance versus S impedance to the equivalent Lambda-Rho versus Mu-Rho crossplots (Goodway, 2001).
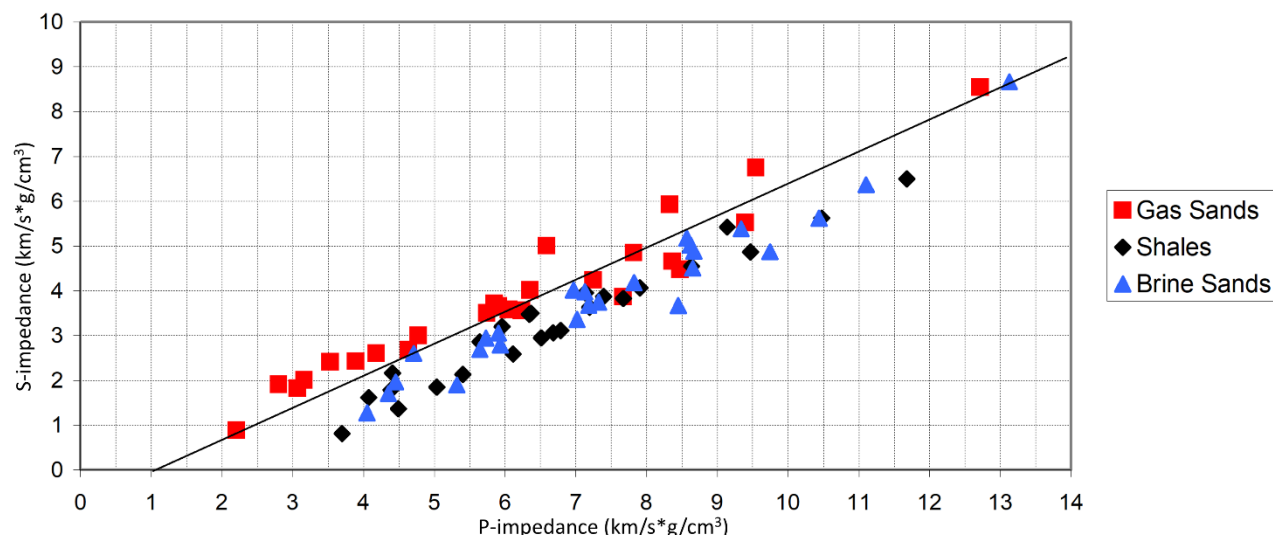

Figure 5*: Crossplot between P-impedance and S-impedance using data on P-velocity, S-velocity and density published by Castagna and Smith (1994).*
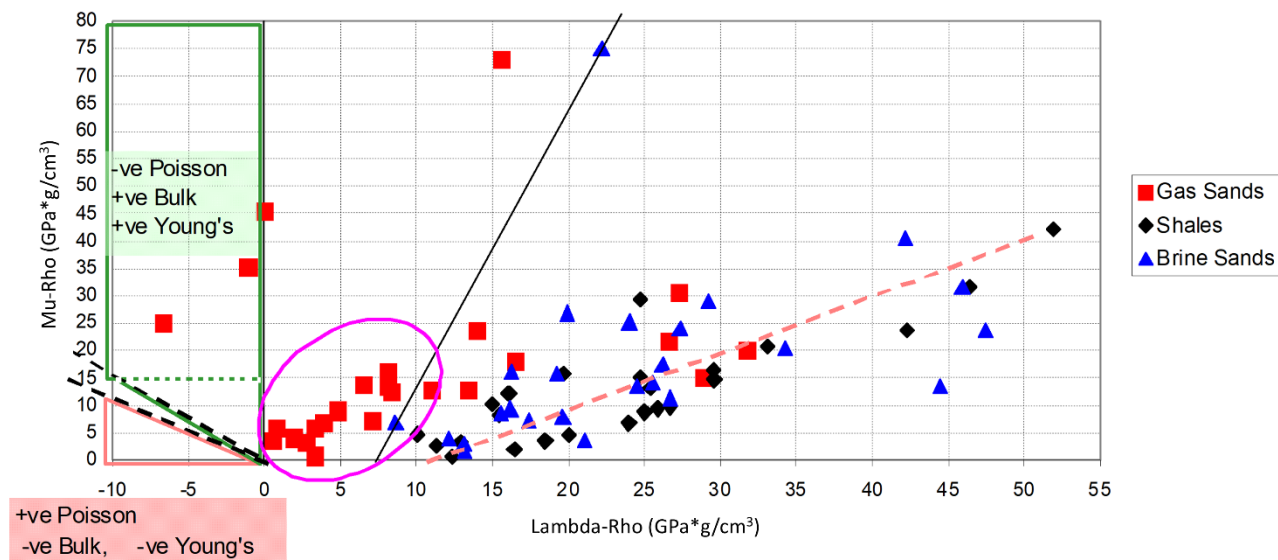

Figure 6*: Crossplot between computed Lambda-Rho and Mu-Rho using the data on P-velocity, S-velocity and density published by Castagna and Smith (1994). Notice the negative values of the elastic constants to the left of the crossplot, which appear to be erroneous.*

A couple of interesting observations can be made by comparing the cross-plots:

a) The Lambda-Rho versus Mu-Rho crossplot (Figure 6) provides a better separation of the gas sands from brine sands and shales within the fully available crossplot space, making it more effective for lithology, fluid characterisation and most importantly, error identification. This is not the case for the equivalent impedance crossplot (Figure 5) that shows a strong narrow correlation between P-impedance (Ip) and S-impedance (Is) for all rock types leading to relationships such as Castagna's "mudrock line" (dark black solid lines show cut-offs for gas sand separation on both crossplots). The reason for this strong Ip to Is correlation stems from the same ambiguity between V_P and V_S that share the shear modulus Mu, as shown in the velocity relationship equality; $V_P^2 = \lambda/rho + 2V_S^2$. By contrast the Lambda-Rho and Mu-Rho values are fundamentally more orthogonal giving rise to both tight clusters of similar lithologies (lower left quadrant gas sands as circled) as well as distinctly separated linear relationships for background brine sands and shales (dashed orange line).

b) The Lambda-Rho and Mu-Rho crossplot offers a more intuitive interpretation and error analysis/identification of these rock types, where the circled low Mu-Rho gas sands are most likely younger, less consolidated sands than the three gas sand values that appear well separated in the upper left quadrant with mid-to high Mu-Rho values. However, these three isolated points are clearly erroneous having either zero or negative Lambda and Poisson ratio values, but positive bulk modulus. This compounds the error, as these sand log values could be used for modelling by Gassmann fluid substitution without recognizing the possibility that the logs might be in error. Even further confusion could arise if any of the low Mu-Rho gas sands were to fall in the negative Lambda region shown by the lower left orange triangle. In this case, Poisson's ratio would be positive and believable while the bulk modulus, Young's modulus and Lambda would be negative. Therefore, a conclusion from the Lambda-Rho, Mu-Rho cross-plot mapping of the confusing positive to negative non-linear behaviour for bulk, Young's moduli and Poisson's ratio within the clearly consistent negative Lambda region, is that Lambda alone represents the material's true incompressibility. The other elastic parameters disguise and confound measurement errors, complicating their use in calibrating AVO/QI.
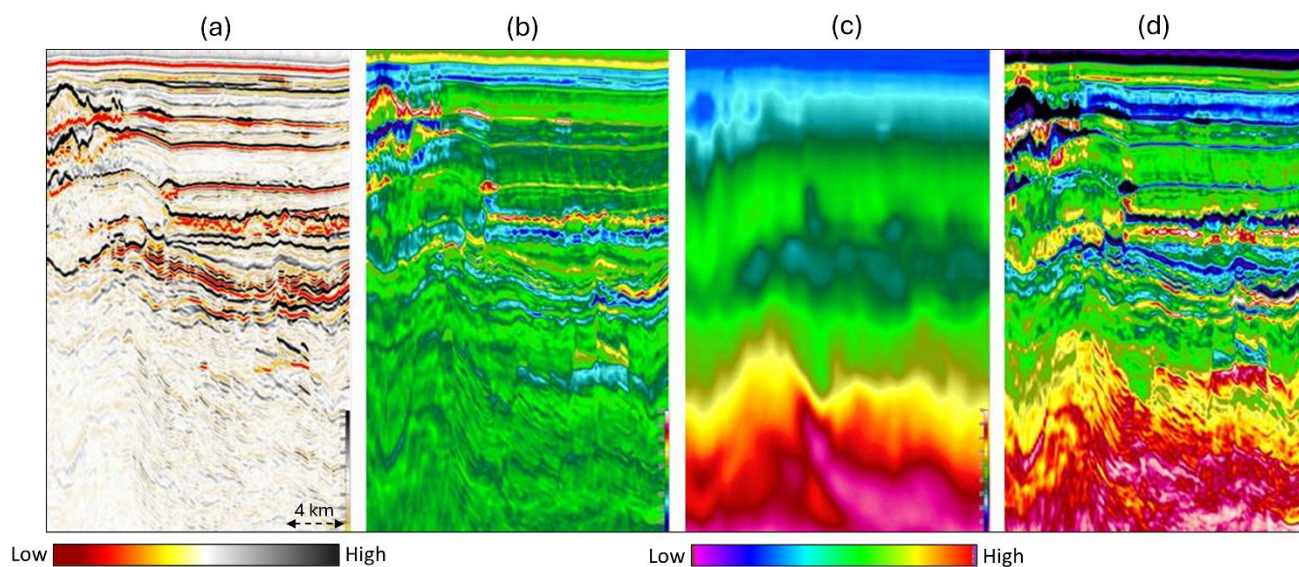

Figure 7: Equivalent segments of a section from the (a) seismic, (b) computed relative acoustic impedance, (c) LFM with FWI input, and (d) computed absolute acoustic impedance volumes. Notice the impact of FWI on LFM building and absolute inversion. (Images courtesy of Andrew Long, PGS)

6

3. Need for correct low frequency models (LFM) for AVO Fluid Factor and QI from relative and absolute Inversion: well log co-kriged migration velocities or FWI velocities.

The critical need for an accurate LFM can be seen in the following steps and absolute inversion application for a general background model workflow.

a) Determine low frequency cutoff and high pass filter seismic data

b) Use same low-pass cutoff filtered logs co-kriged with processing velocity field for LFM building (equivalent proxy FWI see Figure 7c)

c) Estimate wavelets on high pass range frequency data

d) Perform relative inversion on high pass range frequency data

e) Incorporate LFM to produce the full-frequency inversion:

- Use the LFM as background input to the full-frequency band absolute inversion

- Use the LFM to transform the high pass range frequency relative inversion to the absolute inversion

Figure 7 shows the sequential impact and importance of applying an accurate LFM in broadband QI. This process transforms relative inversion to absolute inversion, significantly enhancing resolution when compared to the input seismic data. However, for optimal results, the low pass filtered elastic logs must be sufficiently long and correctly tied to the input seismic data. This ensures that incorporating the LFM with the relative inversion produces the optimal broadband high resolution absolute inversion result as shown in Figure 7d for acoustic impedance (AI). Figure 8 shows the absolute inversion broadband uplift for elastic properties by comparing the inversion tied to log overlays in the left/middle panels for AI, V_P/V_S and Rho with the LFM track shown as a dashed overlay. The last right most mini cross section panels in Figure 8 show a similar optimally calibrated result tied to the respective elastic log tracks.
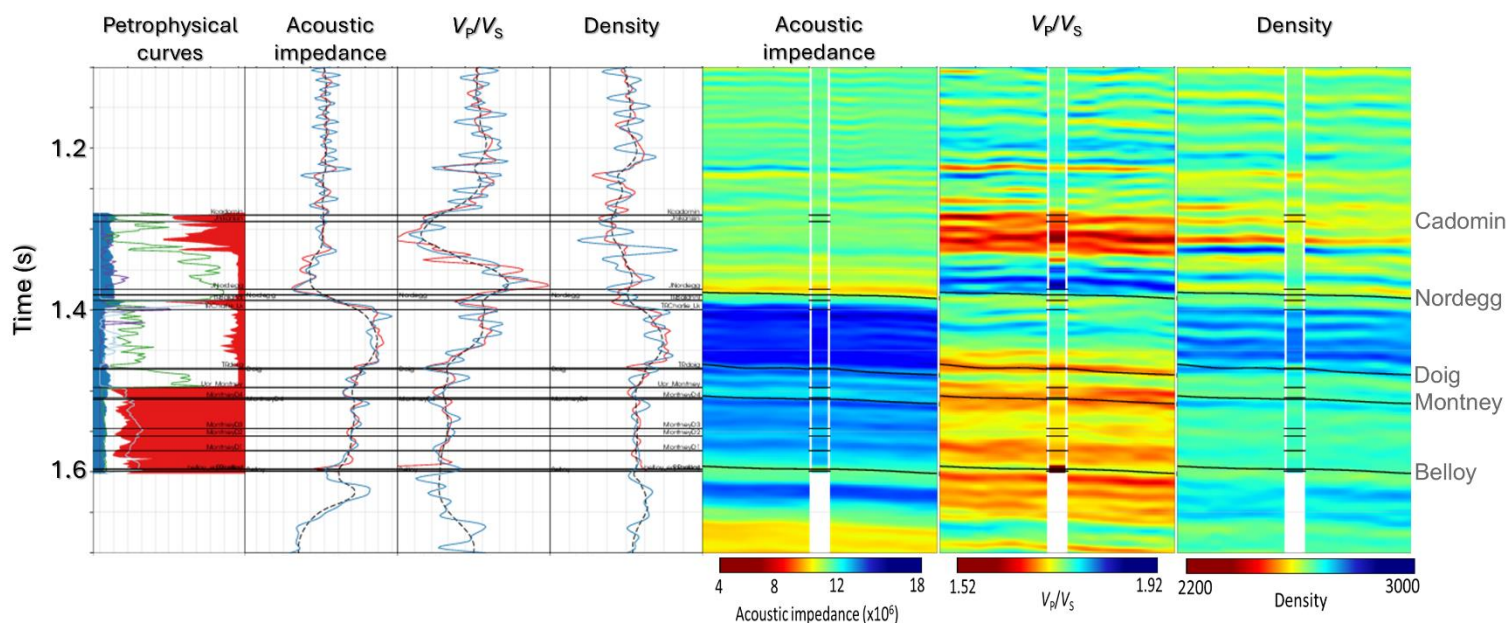

Figure 8: Desired absolute inversion result with use of accurate LFM workflow. Note the uplift from combining the correct LFM with relative inversion for the improved detail and accuracy of the absolute inversion (shown in the inversion (blue) to log track (red) overlays in the left/middle panels for acoustic impedance, V_P/V_S, and density with LFM track as dashed overlay). (After Gordon et al., 2013)

7

The next consideration for an accurate LFM concerns the need for a background model reference in both QI and AVO reflectivity inversion e.g. Fluid Factor (Gidlow et al., 1992; Fatti et al., 1994) as given by $R_P/R_S = (5(V_P - A))/(5V_P - A)$, where R_P and R_S are P and S reflectivities from AVO/QI of relative inversion outputs (Goodway, 2001; Hoffe et al., 2008) and A is the intercept in the Castagna mudrock relation $V_P = A + BV_S$ (Castagna et al., 1985).
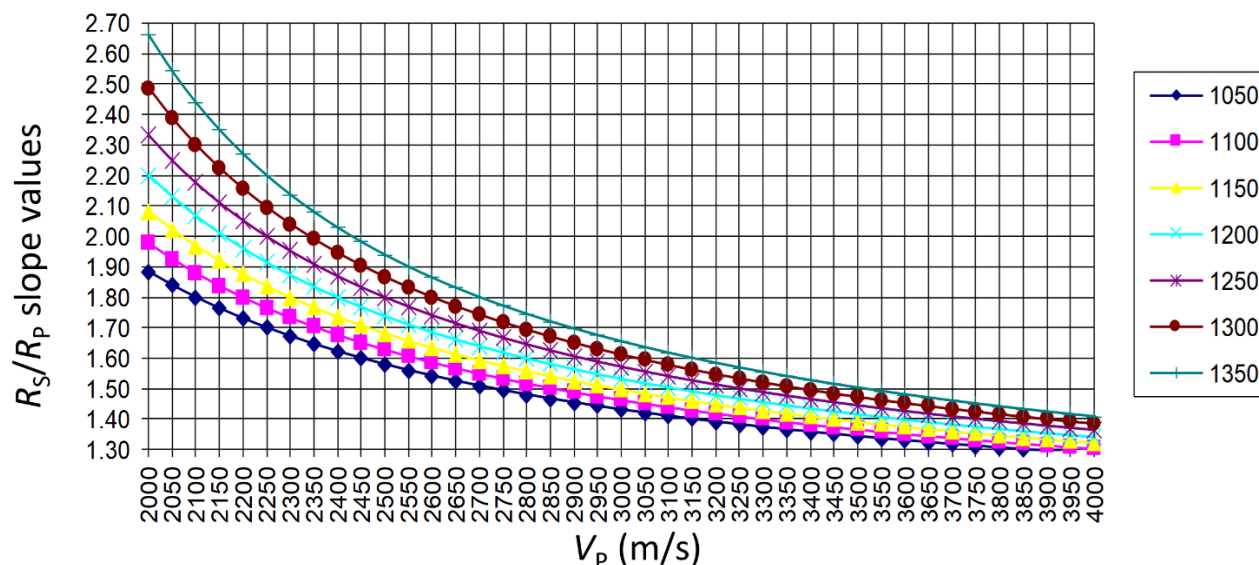

Figure 9: Variation of R_S/R_P slope as a function of interval V_P for varying mudrock line intercept values indicated in the legend. The graph above (based on equation for R_P/R_S in the previous paragraph) shows the variation in the R_S to R_P slope relationships with increasing P velocity's dependence as a function of depth on the shale or wet sand "mudrock line" intercept A (legend) fit that is used.

The advantage of this formulation for a Fluid Factor R_P/R_S ratio factor ff, is that it requires no explicit shear velocity or V_P/V_S ratio and instead just the mudrock line intercept A along with an interval V_P or V_{int} from the V_{rms} PSDM velocity field. The dependence of the R_P/R_S ratio with increasing interval V_P (depth) and mudrock line intercept A from the formulation above, is shown in the graph in Figure 9. One noteworthy observation from this graph is that the R_S/R_P ratios asymptotically converge and reduce with increasing interval V_P (depth), irrespective of mudrock line intercept A.

Another interesting observation regarding the mudrock line-based background LFM for the R_P/R_S Fluid Factor slope ratio is that both the V_S shear "fractional velocity contrasts" and R_S fractional shear impedance contrasts, are theoretically larger than the P-wave R_P equivalents for the same reflector (as noted by Aki & Richards (1980), p154, but no theoretical explanation for this "tendency" is provided).

The mudrock line-based background LFM R_P/R_S factor given above, is useful in defining the AVO Fluid Factor expectation for QI as a time variant function of V_P depth trends obtained from NMO/PSDM interval velocities. This is a critical requirement for creating a dynamic Fluid Factor (FF) QI attribute as FF = R_P – (ff x R_S). This equation defines the background relationship between R_P and R_S so that after removing the background reflectivities the fluid hydrocarbon anomalies are all that remain in the FF section (see Figures 10 and 11). Figures 10a and 11 illustrate the practical application of this QI method. From this, the correct global/background LFM based Fluid Factor discrimination can be tied directly to the seismic R_P and R_S model traces reflectivities that reveal and isolate the local AVO reflectivity anomalies. The model study in Figure 11 demonstrates a successful application of this method for a Mackenzie Delta gas/oil discovery.
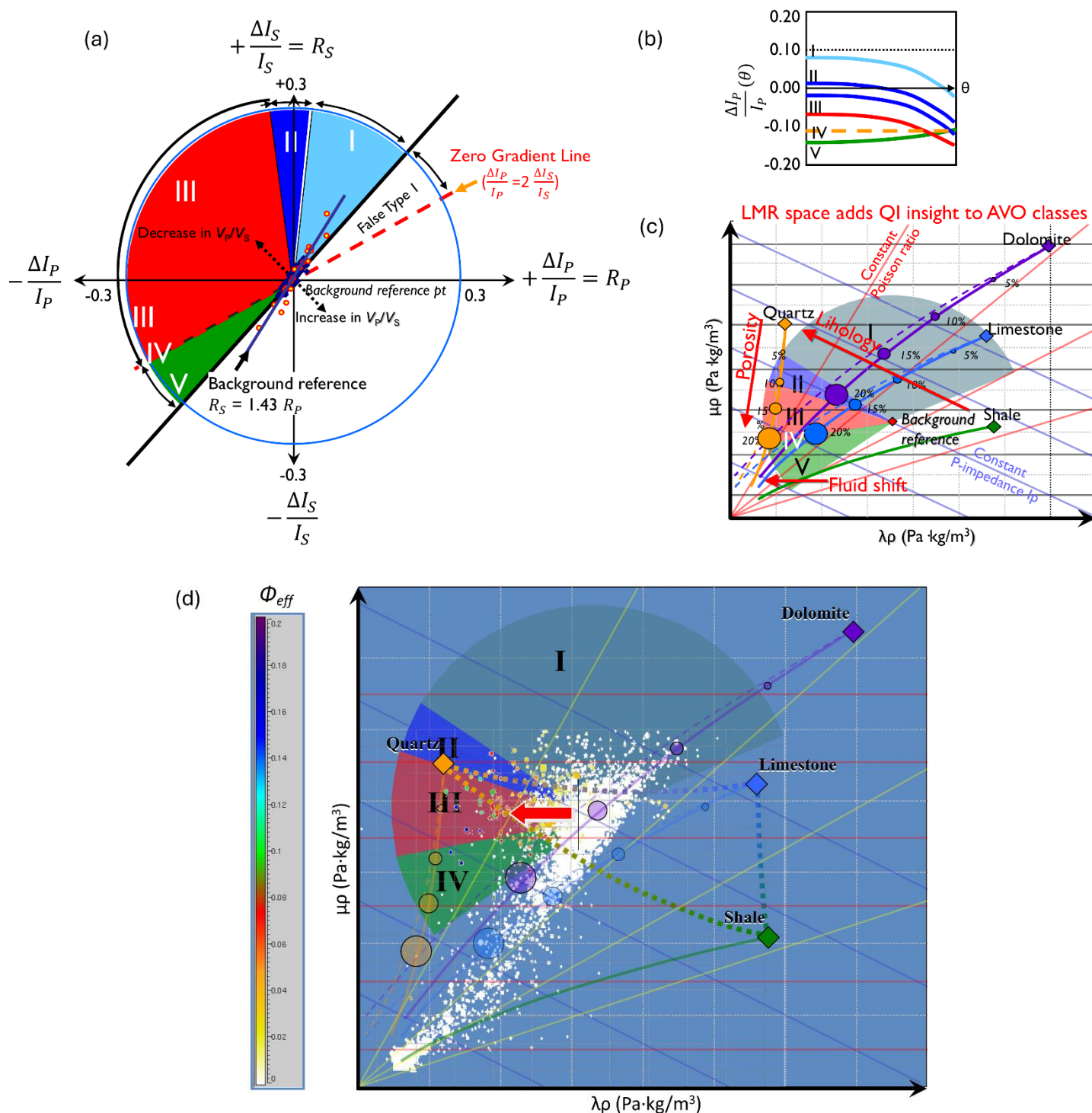
Figure 10: *(a) AVO classes and fluid factor background LFM defined in the AVO reflectivity R_P vs R_S cross-plot space. (Images adapted from Hoffe et al., 2008). (b) AVO classes proposed by Rutherford and Williams (1989), Castagna et al. (1998) and Young and LoPiccolo (2003). (c) AVO classes in LMR crossplot space. (d) The adaptations in (a) and (c) can all be put together in LMR space. More QI insight can be obtained for the AVO classes in LMR space.*
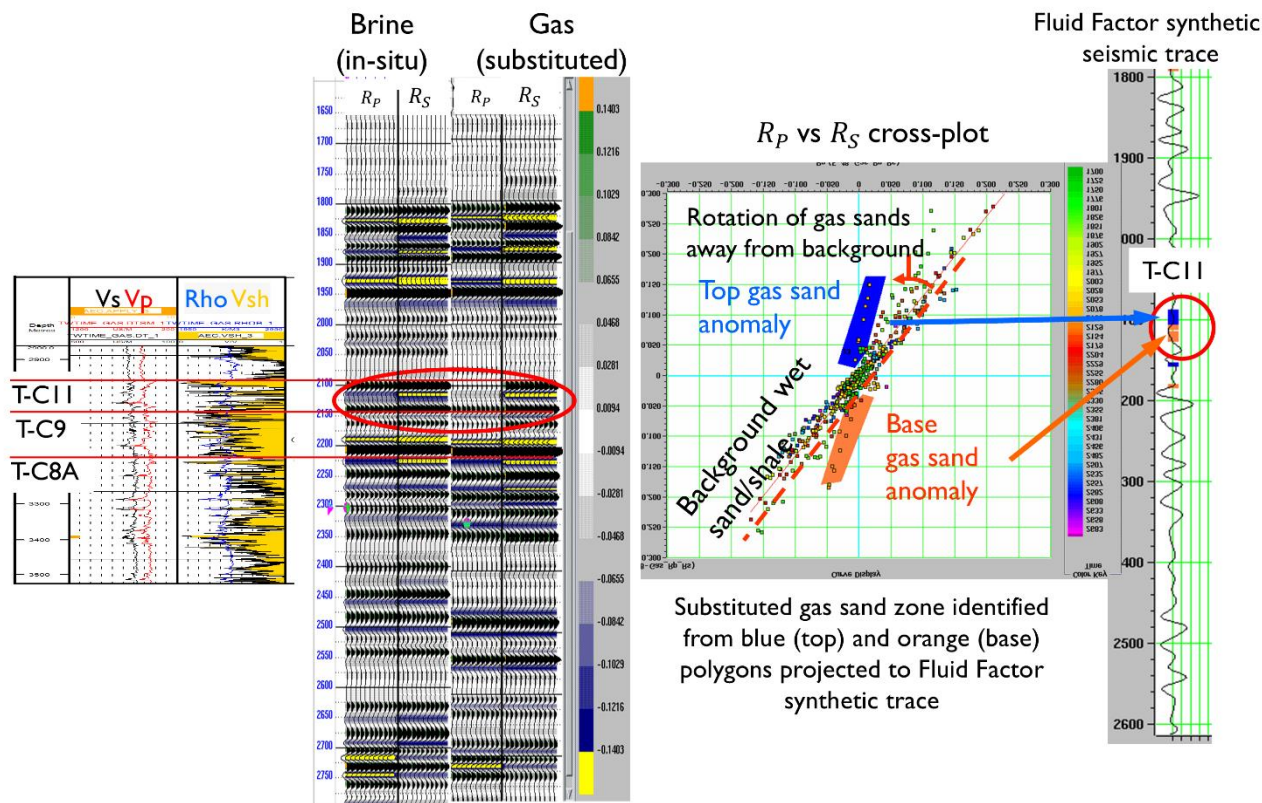
Figure 11: *Pre-drill AVO model reflectivity prediction for R_P, R_S synthetics comprising brine (insitu) versus gas (substituted) to discriminate hydrocarbon zones for a Mackenzie Delta gas/oil discovery.*
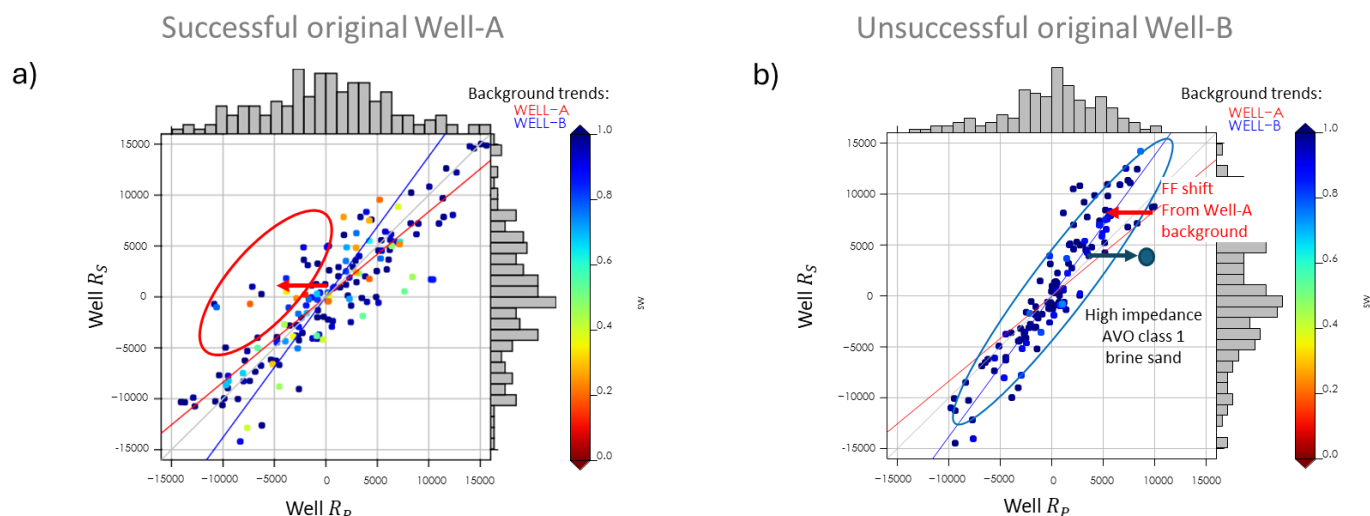

Figure 12: *Fluid Factor R_P vs R_S crossplots for (a) successful, and (b) unsuccessful exploration drilling due to LFM background reference. In (a), a negative fluid factor shift (drop in V_P/V_S) corresponding to gas filled porosity in low impedance sand is seen (indicated by red arrow and oval). In (b), a positive fluid factor shift (increase in V_P/V_S) from fizz-rock mudrock trend is seen. The high impedance sand is the anomaly off the fizz-gas mudrock trend (arrow and dot). Well-A and Well-B background trends DEVIATE for log points in target zone at Well-B as shown by blue oval. Thus, the choice of background trend is critical.*
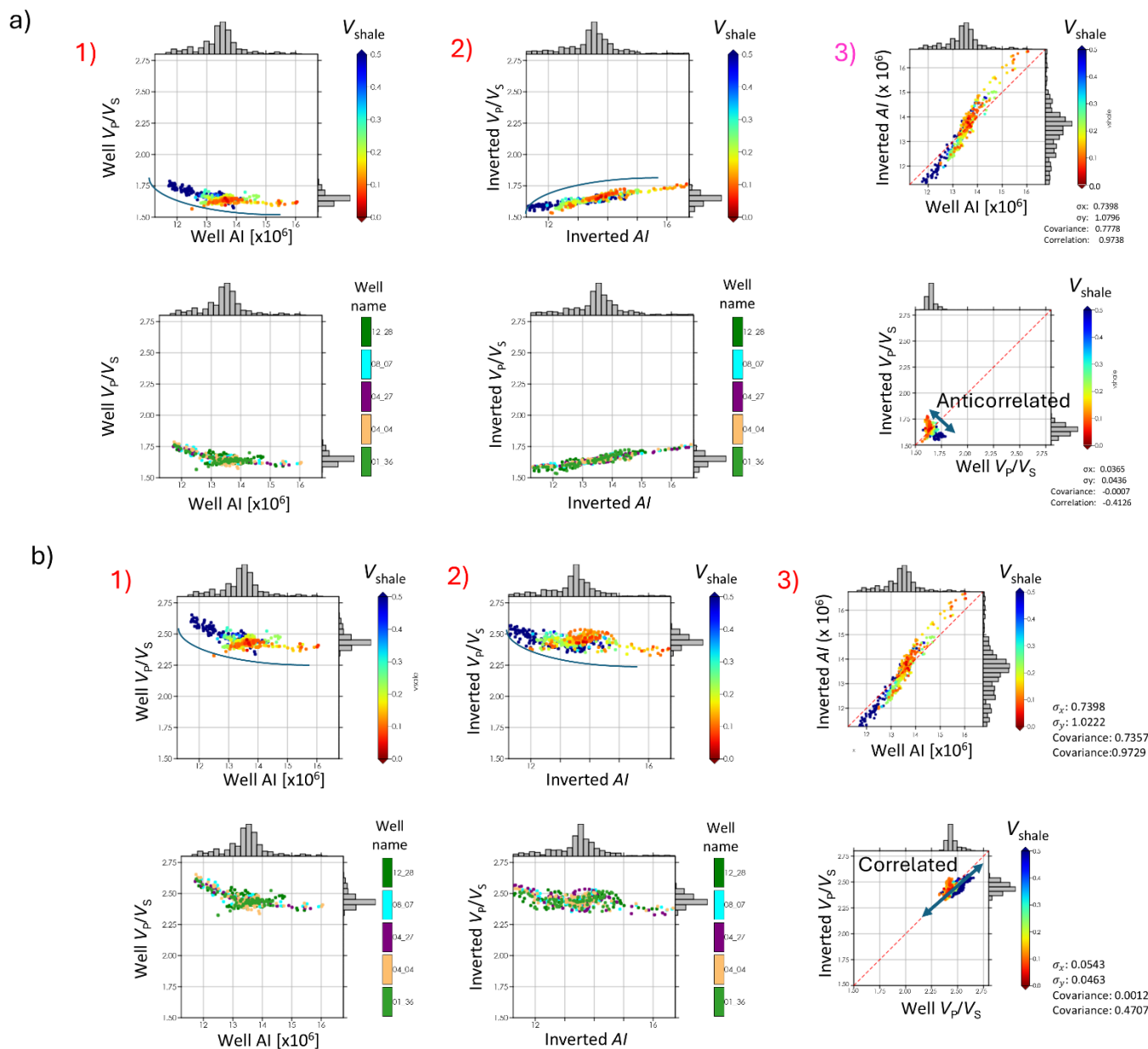
10

Figure 13: *(1) (above) Crossplot of acoustic impedance (AI) versus V_P/V_S using well data colour-coded with V_{shale}, and (below) the same crossplot colour-coded with well name. (2) (above) Crossplot of inverted acoustic impedance (AI) versus inverted V_P/V_S colour-coded with V_{shale}, and (below) the same crossplot colour-coded with well name. (3) (above) Crossplot of inverted acoustic impedance (AI) versus well AI colour-coded with V_{shale}, and (below) crossplot of inverted V_P/V_S versus well V_P/V_S colour-coded with V_{shale}. All crossplot trends used are with (a) **incorrect**, (b) **correct** shale-mudrock background model. The relative inversion results for AI vs V_P/V_S are very sensitive to the background shale-mudrock trend and if this is incorrect, they will have an anti-correlated litho-fluid V_P/V_S trend seen in the middle and right panels compared to the correct log cross-plot V_P/V_S trend in the left panel in the (a) crossplots above. With the correct background shale-mudrock trend, the relative inversion results for AI vs V_P/V_S are correlated to the litho-fluid V_P/V_S trend seen in the middle and right panels compared to the correct log cross-plot V_P/V_S trend in the left panel in the (b) crossplots above.*

11

However, if the background LFM reference model is inaccurate, then identification of hydrocarbons through a local reflectivity anomaly Fluid Factor discrimination will fail. This failure of the method is illustrated in Figure 12 that compares a successful application in Well A with a subsequent unsuccessful Well B.

The background trends for Well A and Well B are the same (converging at the crossplot origin) for log points in the target zone at Well A shown by red circle. Therefore, the choice of background is irrelevant in this case. However, the presence of even low gas saturation (fizz-gas) in high impedance mudrock background brine sands causes the sands to have the same P-impedance as the background shales and hence fits these sands to the Well-B background trend (blue oval for Well B in Figure 12b).

Consequently, if the Well A background trend (red line) were used as the R_P to R_S scalar for the Fluid Factor in Well B, there would be a negative Fluid Factor shift (drop in V_P/V_S) from the Well A background trend. This shift would affect both the low saturation gas sands and all the rest of the Well B background shale trend (blue line and oval).

A relative inversion that might follow from the reflectivity-based Fluid Factor approach, allows for an improved quantitative discrimination between lithology, porosity and fluid effects using Lambda-Rho-Mu-Rho, unlike the Fluid Factor method. The QI of the relative inversion results within the context of the Fluid Factor R_P, R_S analysis is illustrated in Figure 10c for an LMR cross-

plot space template and overlays of AVO classes considered in the Fluid Factor analysis.

However, despite being termed relative, there is a little-known fact about the relative inversion results' need for a correct background reference shale or mudrock trend. The reason for this is that the correct background trend needs to be referenced to make sense of the elastic property discrimination between lithology, porosity and fluid fill for LMR cross-plot template interpretation (Figure 10c). If the background shale-mudrock trend is incorrect then the relative inversion results for AI vs V_P/V_S will have an anti-correlated litho-fluid V_P/V_S trend seen in the middle and right panels of Figure 13a (2) and (3), compared to the correct log cross-plot V_P/V_S trend in the left panel of Figure 13a (1).

A more noticeable impact of using the incorrect shale-mudrock background as reference for relative inversion AI, V_P/V_S and Rho outputs can be seen in the log and inverted seismic track overlays and mini-sections tied to calibrated background logs in Figure 14a (incorrect model) compared to Figure 14b (correct model).

In Figure 14a, using the incorrect background refence model, the V_P/V_S inversion overlay is anticorrelated with the log track, which is typically observed in most relative inversion results. Additionally, there is no correlation for Rho. By contrast in Figure 14b, when the correct shale-background reference is used, the V_P/V_S inversion overlay is now correlated and aligned with the log track, and the Rho tracks show an improved correlation.
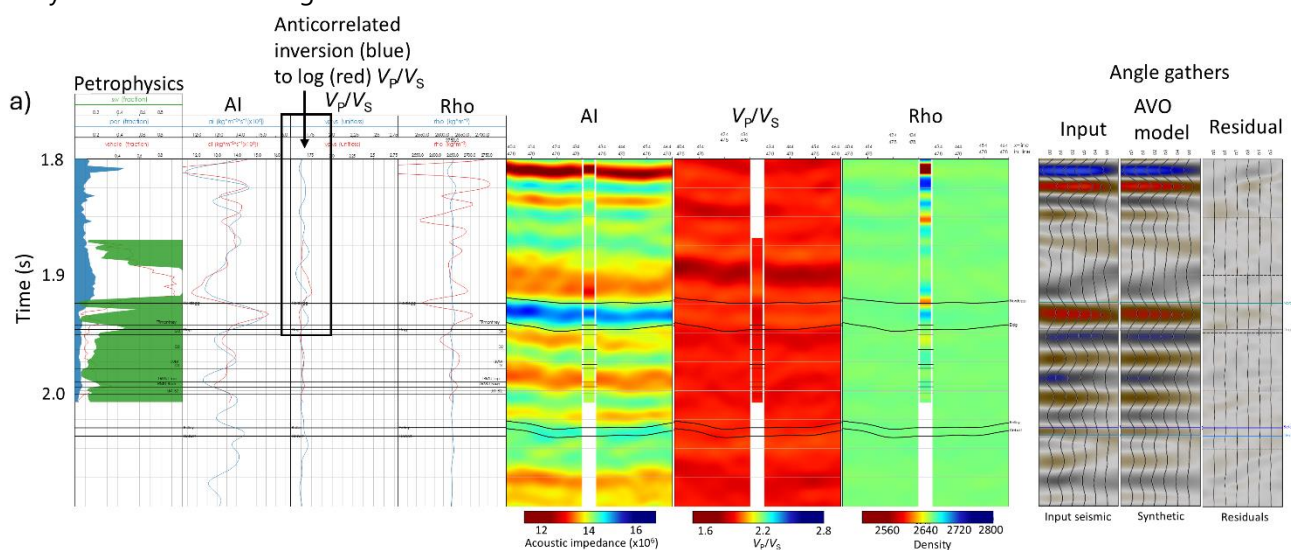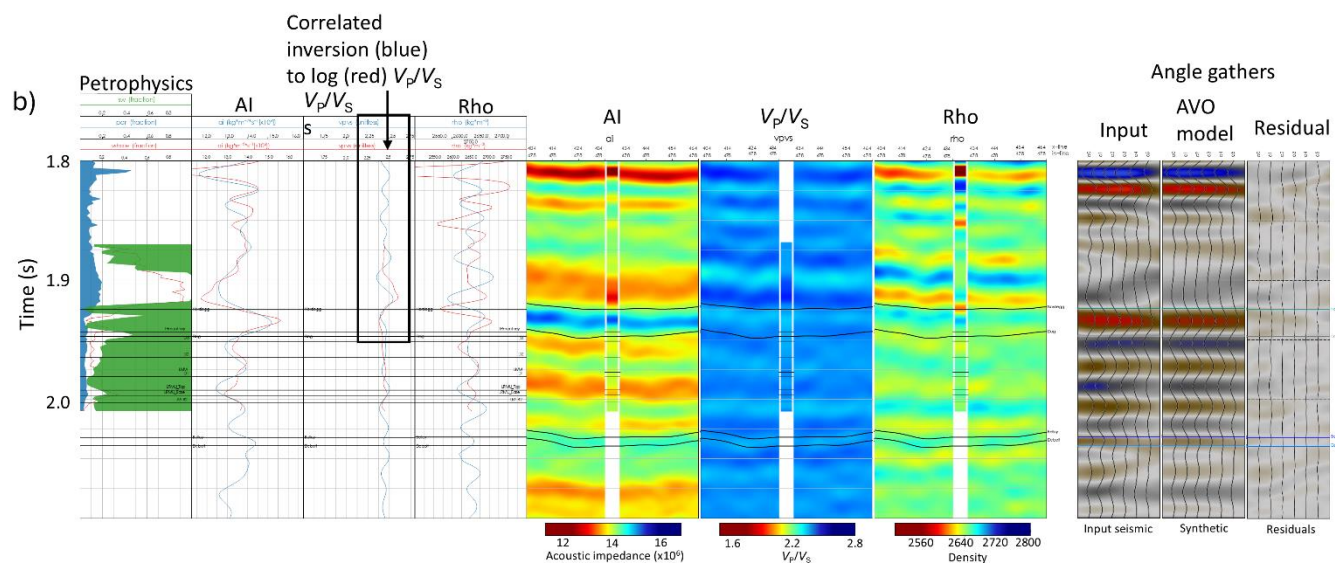
Figure 14: Relative Inversion AI and V_P/V_S calibrated to logs comparing filtered log (red track) to inversion result (blue track) for AI, V_P/V_S and rho with (a) incorrect, and (b) correct shale-mudrock background model. The Relative Inversion result for V_P/V_S is very sensitive to the background shale-mudrock trend and if this is incorrect, it will have an anti-correlated litho-fluid V_P/V_S trend seen in the middle panels' inversion (blue) to log (red) overlays. With the correct background shale-mudrock trend, the Relative Inversion result for V_P/V_S (blue overlay) is correlated to the litho-fluid V_P/V_S trend seen in the middle panels compared to the correct log V_P/V_S overlay (red).
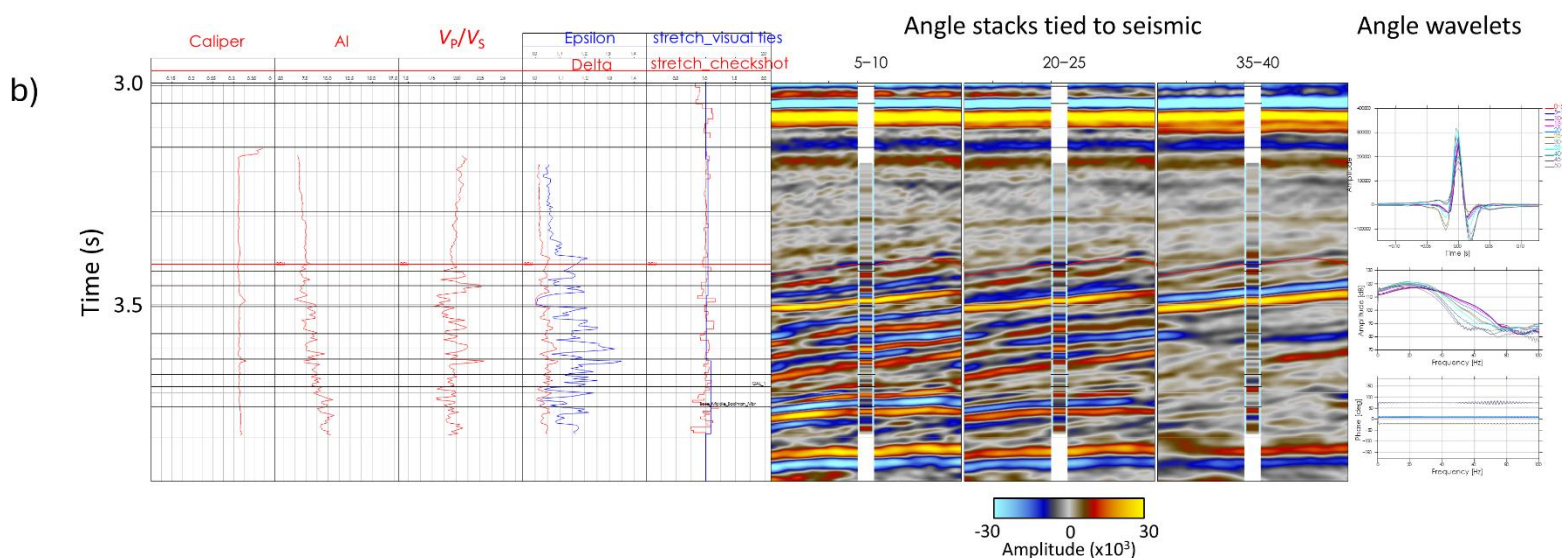
13
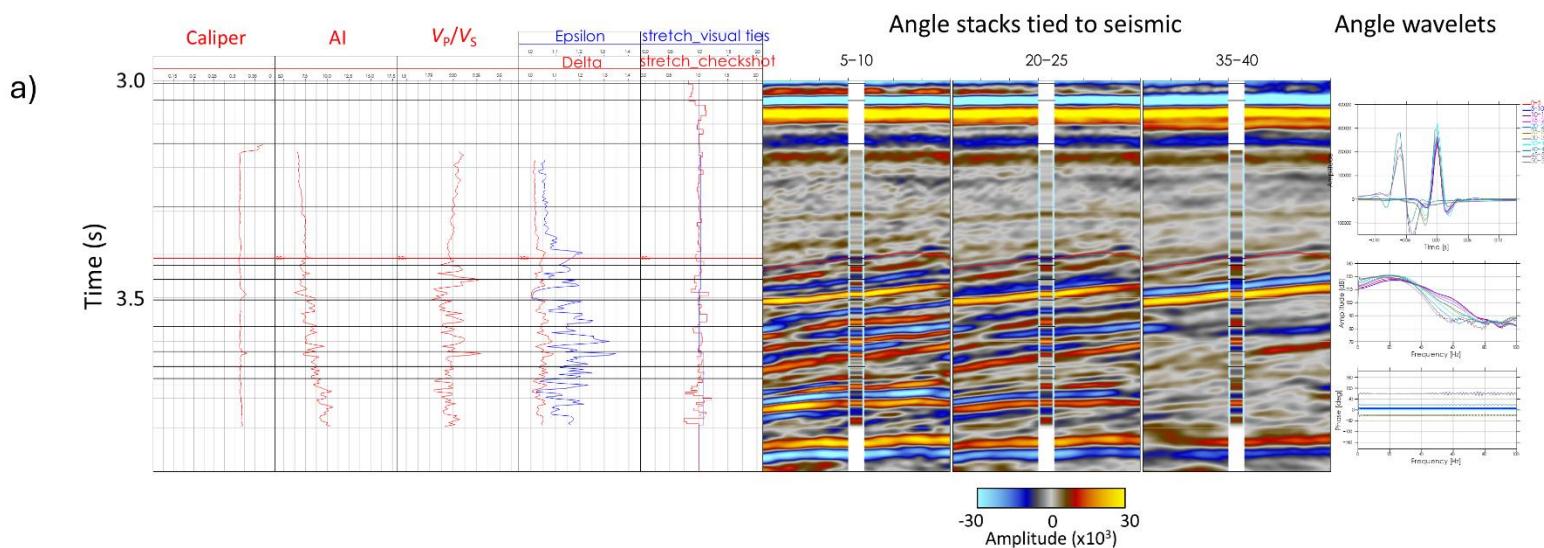
Figure 15: *Angle stack ties and wavelet estimate QC for an (a) isotropic synthetic seismogram model, and (b) anisotropic synthetic seismogram model. A standard result of the isotropic approach to angle dependent wavelet estimates is shown in figure panels (Figure 15a). Typically, the higher angle wavelets are mis-tied and inconsistent with the other angle wavelets that have comparably stable spectral phase with the expected amplitude decay with increasing angle. Accounting for VTI effects in the synthetic models' encasing shale requires anisotropic VTI log or seismic NMO measurements of Thomsen's delta and epsilon parameters. Once these parameters are used to generate a VTI synthetic angle forward model, then the extracted far angle wavelets are now seen to be consistent and a stable match to the other near to mid angle range wavelets as shown in the Figure 15b panels and unlike the isotropic model case in Figure 15a above.*

4. Wavelet estimation including VTI- spectral (amplitude and phase) log tie and wavelet spatial estimation/stability especially for phase

This final section concerns a relatively unknown and often overlooked issue: the optimal angle wavelet ties for background shales with VTI anisotropy. A fundamental requirement in any pre-stack inversion is the need to accurately estimate and compensate for the bandlimited amplitude and phase of angle dependent wavelets that arise from frequency dispersion and absorption due to wave propagation. This is typically done by using vertical elastic logs to generate a forward angle synthetic model that ties to the seismic angle sub-stacks. Because there are no measurements of anisotropy in the input logs, the resulting forward angle synthetic model is isotropic.

A standard result of this isotropic approach to angle dependent wavelet estimates is shown in Figure 15a. Typically, the higher angle wavelets often mistie and become inconsistent with the wavelets at other angles, which usually display stable spectral phase and expected amplitude decay with increasing angle. This inconsistency, particularly in the higher angle range, is visible in both the angle limited mini section ties (for angle ranges of 5°-10°, 20°-25° and 35°-40°) in the middle panels and the right panel, which shows the estimated angle range wavelets. The phase of the higher angle wavelets is clearly distorted and misaligned compared with the near and mid angle wavelets.

Consequently, in many AVO inversion projects, the far angle input data are often rejected, under the assumption that the amplitudes and AVO at the farthest angles are flawed due to many factors that include noise/multiple interference, wave propagation attenuation, inadequate processing, etc. What is rarely questioned, however, is the adequacy and appropriateness of the log-based forward model used to create the angle synthetics for the wavelet extraction. However, this angle dependent wavelet mistie suggests that the issue may lie with the synthetic model, which

14

does not account for an anisotropic VTI shale background. In order to account for these VTI effects in the synthetic models' encasing shale, requires anisotropic VTI log or seismic NMO measurements of Thomsen's delta and epsilon parameters. Once these parameters are used to generate a VTI synthetic angle forward model, the extracted far angle wavelets are now seen to be consistent and a stable match to the other near- to mid-angle range wavelets is seen as shown in Figure 15b.

CONCLUSIONS

Regarding the question of whether QI is merely a buzzword or is being effectively implemented in our industry, I believe that in the context of AVO inversion, effective QI can be achieved by incorporating additional underutilized supplementary data. This data is essential for correlation, calibration, and integration, and is crucial for successfully applying AVO/QI workflows. These include, the walkaway VSP AVO and elastic logs for combined borehole and surface seismic inversion after utilizing the VSP guided background offset scaling/balancing, the use of error free elastic log suite for AVO calibration and rock physics modeling, using an accurate LFM is required for performing AVO inversion and deriving the elastic properties therefrom, and finally, the use of accurate angle-dependent wavelets is required for AVO impedance inversion, usually extracted under an isotropic assumption, and which falls short of accounting for the background shales with VTI anisotropy. I contend, and strongly recommend, that if additional data, as discussed above for AVO inversion, are brought into the QI exercises, their performance can be made effective, which can add significantly to the bottom-line of oil and gas companies. $\mathcal{G}$

REFERENCES

Aki, K., and P. G. Richards, 1980, Quantitative Seismology, W. H. Freeman & Co.

Castagna, J. P., M. L. Batzle, R. L. Eastwood, 1985, Relationships between compressional-wave and shear-wave velocities in clastic silicate rocks, Geophysics, **50**, no. 4, 571–581. https://doi.org/10.1190/1.1441933

Castagna J.P., and S. W. Smith, 1994, Comparison of AVO indicators: a modelling study, Geophysics, **59**, no. 12, 1849-1855. https://doi.org/10.1190/1.1443572

Castagna J.P., and H. W. Swan, 1997, Principles of AVO crossplotting, The Leading Edge, **16**, no. 4, 337-342. https://doi.org/10.1190/1.1437626

Castagna, J. P., H. W. Swan, and D. J. Foster, 1998, Framework for AVO gradient and intercept interpretation, Geophysics, **63**, no. 3, 948-956. https://doi.org/10.1190/1.1444406

Coulombe, C. A., R. R. Stewart, and M. J. Jones, 1996, AVO processing and interpretation of VSP data, Can. J. Expl. Geophys., **32**(1), 41-62.

Downton J., W. Goodway, and T. Chen, 1999, Quantitative comparison of deriving P and S impedances from PP and PS surface and VSP dat a, CSEG National Convention Expanded Abstracts.

Fatti J. L., G. C. Smith, P. J. Vail, P. J. Strauss, and P. R. Levitt, 1994, Detection of gas in sandstone reservoirs using AVO analysis: A 3D seismic case history using the Geostack technique, Geophysics, **59**, no. 9, 1362-1376. https://doi.org/10.1190/1.1443695

Gidlow, P. M, G. C. Smith, and P. J. Vail, 1992, Hydrocarbon detection using fluid factor traces; A case history, SEG/EAEG Summer Workshop, 78-79.

Goodway W., T. Chen, and J. Downton, 1997, Improved AVO fluid detection and lithology discrimination using Lamé parameters; $\lambda\rho$, $\mu\rho$ and λ/ρ fluid stack from P and S inversions, CSEG National Convention Expanded Abstracts, 148-151.

Goodway, W., T. Chen, and J. Downton, 1998, Joint P-P and P-S inversion of a walkaway VSP for V_P, V_S and V_P/V_S compared to log data and for surface P-P calibration and inversion, SEG Post-Convention Workshop on 'Can P-wave AVO be quantitative or do we need multi-component'.

Goodway W., 2001, AVO and Lamé constants for rock parameterization and fluid detection, CSEG Recorder, page numbers here please.

Gordon, A., E. Mutual, R. Cova, S. Leaney, B. Goodway, W. Pardasie, M. Ng, 2013, Characterization of multiple formations for gas production and CO_2 sequestration, GeoConvention, 1-4.

Hoffe, B. H., M. A. Perez, and W. Goodway, 2008, AVO interpretation in LMR Space: A Primer, CSEG Annual Convention, Expanded Abstracts.

Rutherford, S. R. and R. H. Wiliams, 1989, Amplitude-versus-offset variations in gas sands: Geophysics, **54**, no. 6, 680-688. https://doi.org/10.1190/1.1442696

Smith, G.C, and P. M., Gidlow, 1987, Weighted stacking for rock property estimation and detection of gas, Geophysical Prospecting, **35**, no. 9, 993-1014. https://doi.org/10.1111/j.1365-2478.1987.tb00856.x

Young, R. A. and R. D. LoPiccolo, 2003, A comprehensive AVO classification: The Leading Edge, **22**, no. 10, 1030-1037. https://doi.org/10.1190/1.1623645

BIOGRAPHY

Bill Goodway obtained a B.Sc. in Geology from University College London and a M.Sc. in Geophysics from University of Calgary. After working in the UK, he joined PanCanadian Petroleum in 1985 becoming Team Lead of a Seismic Analysis Group and Advisor for Seismic Analysis at Encana. In 2010 he became Manager Geophysics-Advisor Senior Staff at Apache, involved in seismic acquisition design, processing interaction, experimental special projects and new AVO methods. Bill is currently Qeye's Scientific Advisor Quantitative Interpretation and AVO technology.

Bill has authored numerous papers at CSEG, EAGE and SEG conventions on seismic acquisition design, processing, borehole geophysics, anisotropy, multicomponent recording and QI/AVO.

He was awarded four CSEG Best Paper Awards, the CSEG Medal and was a past SEG Honorary Lecturer for North America. The CSEG recognized Bill as the 2013 Symposium honouree and in 2016 he received the SEG's Reginald Fessenden Award for lambda-rho-mu (LMR) inversion technology.